

# MODELING OF AN OBLIQUE INCIDENT P1-WAVE IN A WATER SATURATED SOIL WITH THE WAVE BASED METHOD

M. LAINER AND G. MÜLLER

Chair of Structural Mechanics  
Technical University of Munich  
Arcisstrasse 21, 80333 Munich  
e-mail: mirjam.lainer@tum.de, gerhard.mueller@tum.de  
web page: www.cee.ed.tum.de/bm

**Key words:** Wave Based Method, Biot's theory, Oblique incident wave

**Abstract.** In this contribution, a coupling approach between the Wave Based Method and an oblique incident P1-wave is presented. The approach is used to model a poroelastic halfspace with an empty canyon by applying *Biot's* theory for low frequencies. The system's response is compared with a reference solution from literature. Moreover, a second coupling approach is introduced to permit the modeling of a filled canyon. In the special case of a canyon filled with the material of the surrounding soil, the simulation results are compared with the underlying analytical solution.

## 1 INTRODUCTION

Due to irregularities at the surface of a soil, oblique incident wave fronts may cause amplifications of displacements and stresses [1, 2]. To model these for a water saturated soil in the 2D case, it is necessary to consider two irrotational potentials (P1- and P2-wave) and one solenoidal potential (S-wave). The Wave Based Method (WBM) permits to model poroelastic soil for a harmonic loading efficiently, which has already been shown for a surface loading [3]. The WBM belongs to the family of indirect *Trefftz* methods and uses weighted wave functions to approximate the wave potentials of a boundary value problem. Amongst other advantages of the WBM, this numerical method is chosen as it needs significantly less degrees of freedom than a finite element approach [4]. This saves computational time, especially for the approximation of an infinite poroelastic soil medium. The following contribution focuses on the modeling of an incident P1-wave, which excites a poroelastic halfspace with a trapezoidal canyon. That canyon is considered to be empty or filled.

## 2 GOVERNING EQUATIONS AND NUMERICAL MODEL

### 2.1 *Biot's* theory for a fully saturated halfspace

Given is a two-dimensional fully saturated continuum with a solid phase displacement field  $\mathbf{u}^s = [u_x, u_y]^T$  and a fluid seepage field  $\mathbf{U} = [U_x, U_y]^T$ . The fluid seepage field corresponds

to the relative displacements between the enclosed fluid and the solid skeleton, weighted by the porosity  $n^f$ .

$$\mathbf{U} = n^f(\mathbf{u}^f - \mathbf{u}^s) \quad (1)$$

The displacement fields  $\mathbf{u}^s$  and  $\mathbf{U}$  are expressed by the superposition of the two gradients ( $\nabla = [\partial/\partial x, \partial/\partial y]$ ) of the irrotational potentials  $\Phi_{p_1}$ ,  $\Phi_{p_2}$  and the curl ( $\tilde{\nabla} = [\partial/\partial y, -\partial/\partial x]$ ) of the solenoidal potential  $\Psi_s$ , based on *Biot's* theory [5]. These potentials are also called P1-, P2- and S-wave within this publication.

$$\mathbf{u}^s = \nabla\Phi_{p_1} + \nabla\Phi_{p_2} + \tilde{\nabla}\Psi_s \quad (2)$$

$$\mathbf{U} = \gamma_{p_1}\nabla\Phi_{p_1} + \gamma_{p_2}\nabla\Phi_{p_2} + \gamma_s\tilde{\nabla}\Psi_s \quad (3)$$

The parameters  $\gamma_{p_{1/2}}$  and  $\gamma_s$  in Equation (3) correspond to the eigenvalues of the two dynamic equations according to *Biot's* theory [5]. These dynamic equations are simplified, either for  $\nabla\Phi_{p_{1/2}}$  or  $\tilde{\nabla}\Psi_s$  and solved for  $\gamma_{p_{1/2}}$  and  $\gamma_s$ . The wave numbers for the P1-, P2- and S-wave are computed with the material parameters given in Table 1 and for the radial excitation frequency  $\omega = 2\pi f$ , with the frequency  $f$ .

$$k_{p_{1/2}} = \sqrt{\frac{\rho_f + \gamma_{p_{1/2}}\rho_{f2}}{(\alpha + \gamma_{p_{1/2}})M}} \cdot \omega, \quad k_s = \sqrt{\left(1 + \gamma_s \frac{\rho_f}{\rho}\right) \frac{\rho}{\mu}} \cdot \omega \quad (4)$$

$$\text{with } \rho_{f2} = \frac{\rho_f a_t}{n^f} - \frac{i\xi}{\omega(n^f)^2}, \quad \xi = \frac{\rho_f \cdot (n^f)^2}{k_c} \cdot 9.81\text{m/s}^2, \quad k_c = \frac{\kappa_I \cdot \rho_f}{\eta_f} \cdot 9.81\text{m/s}^2$$

With  $\rho_{f2}$  the coupling between fluid and solid phase is expressed. Its real part depends on the tortuosity  $a_t$  and takes into account the effect of the microvelocity field of the fluid phase within the solid skeleton. The imaginary part of  $\rho_{f2}$  is computed with the dissipation coefficient  $\xi$ , which is related to the viscous damping in the medium due to the relative displacement field between fluid and solid phase. The dynamic viscosity  $\eta_f$  and the intrinsic permeability  $\kappa_I$  are decisive for this viscous damping and are used to compute the hydraulic conductivity  $k_c$ .

The Equation (5) shows the formulation of the strain field within a poroelastic medium, which involves the displacement fields given by the Equations (2) and (3). The value  $\zeta$  is introduced, which describes the divergence of the fluid seepage field, or respectively, the amount of fluid leaving the pores. With this formulation of the strain fields, the constitutive Equation (6) is defined for the total stresses, which also involves the description of the total fluid stresses  $\sigma_f$ . The total stresses depend on the two *Lamé* coefficients  $\lambda$  and  $\mu$  as well as the two *Biot* coefficients  $M$  and  $\alpha$ .

$$\begin{pmatrix} \varepsilon_{xx} \\ \varepsilon_{yy} \\ \gamma_{xy} \\ \zeta \end{pmatrix} = \begin{bmatrix} \frac{\partial}{\partial x} & 0 & 0 & 0 \\ 0 & \frac{\partial}{\partial y} & 0 & 0 \\ \frac{\partial}{\partial y} & \frac{\partial}{\partial x} & 0 & 0 \\ 0 & 0 & \frac{\partial}{\partial x} & \frac{\partial}{\partial y} \end{bmatrix} \begin{pmatrix} u_x \\ u_y \\ U_x \\ U_y \end{pmatrix} \quad (5)$$

$$\begin{pmatrix} \sigma_{xx} \\ \sigma_{yy} \\ \tau_{xy} \\ \sigma_f \end{pmatrix} = \begin{bmatrix} \lambda + 2\mu + \alpha^2 M & \lambda + \alpha^2 M & 0 & \alpha M \\ \lambda + \alpha^2 M & \lambda + 2\mu + \alpha^2 M & 0 & \alpha M \\ 0 & 0 & \mu & 0 \\ \alpha M & \alpha M & 0 & M \end{bmatrix} \begin{pmatrix} \varepsilon_{xx} \\ \varepsilon_{yy} \\ \gamma_{xy} \\ \zeta \end{pmatrix} \quad (6)$$

Here, the underlying *Young's* E-Modulus is expressed as a complex value  $E[1 + i\eta]$ , with  $i = \sqrt{-1}$  and the loss factor  $\eta$ .

## 2.2 Description of a poroelastic halfspace with the Wave Based Method

The displacement field from the Equations (2) and (3) are approximated by  $\hat{\mathbf{u}}^s$  and  $\hat{\mathbf{U}}$ , which are described by the Wave Based Method (WBM). The two irrotational potentials and the solenoidal potential are expressed by a sum of weighted wave functions  $\Phi_{p_1,i}$ ,  $\Phi_{p_2,j}$  and  $\Psi_{s,k}$ . These are defined for convex domains and are given by [6].

$$\mathbf{u}^s \cong \hat{\mathbf{u}}^s = \sum_{i=1}^{n_{p_1}} c_{p_1,i} \nabla \Phi_{p_1,i} + \sum_{j=1}^{n_{p_2}} c_{p_2,j} \nabla \Phi_{p_2,j} + \sum_{k=1}^{n_s} c_{s,k} \tilde{\nabla} \Psi_{s,k} \quad (7)$$

$$\mathbf{U} \cong \hat{\mathbf{U}} = \sum_{i=1}^{n_{p_1}} \gamma_{p_1} c_{p_1,i} \nabla \Phi_{p_1,i} + \sum_{j=1}^{n_{p_2}} \gamma_{p_2} c_{p_2,j} \nabla \Phi_{p_2,j} + \sum_{k=1}^{n_s} \gamma_s c_{s,k} \tilde{\nabla} \Psi_{s,k} \quad (8)$$

The minimum number of wave functions  $(n_{p_1}, n_{p_2}, n_s)$  depends on the largest physical wave number  $k$ , respectively the slowest body wave, in the problem domain. The highest wave number in a wave function set must be larger than the truncated wave number  $k$  [4].

$$k_{\bullet}^{\max} \geq T \cdot k, \quad \bullet \in \{p_1; p_2; s\} \quad (9)$$

The truncation factor  $T \in [1; 6]$  is chosen by the user and set to  $T = 2$  for the simulation results presented in this contribution, compare also [6].

The unknowns  $c_{p_1,i}$ ,  $c_{p_2,j}$  and  $c_{s,k}$  in the Equations (7) and (8) are derived within a weighted residual *Galerkin* approach. A boundary value problem, as depicted for example in Figure 1, is split into convex subdomains and boundary conditions are formulated. These are for example *Neumann* ( $\Gamma_\sigma$ ), coupling ( $\Gamma_{(\alpha,\beta)}$ ), mixed ( $\Gamma_{SE}$ ) and absorbing ( $\Gamma_Z$ ) boundary conditions. A precise definition of the wave functions, boundary conditions, resulting stiffness matrices and load vectors, that contribute to the final system of linear equations, can be found in [3].

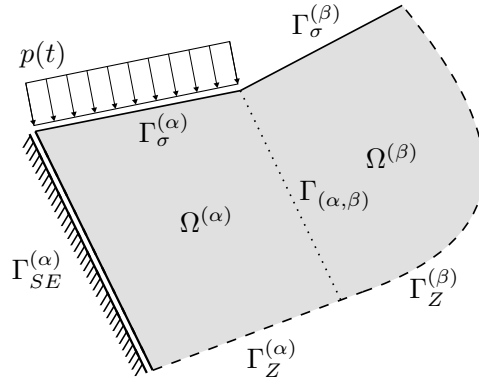


**Figure 1:** Problem with two WB elements

### 3 COUPLING PROCEDURE

#### 3.1 Modified *Neumann* boundary condition

Given is a halfspace with an empty canyon, exposed to an oblique incident P1-wave. As illustrated in Figure 2 (a), the 2D halfspace is fully saturated and described by a finite structure consisting of five WB elements. To approximate the *Sommerfeld* radiation condition, absorbing boundaries are installed along the outer edges. These are illustrated with dotted-straight lines. They permit the transmission of normal incident wave fronts from the scattered wave field, and may cause spurious reflections for non-normal wave fronts, see also [7]. The surface of the halfspace is unloaded and captured by a *Neumann* boundary condition. The surface of the canyon  $\Gamma_\sigma^*$  is also unloaded and related to a modified *Neumann* boundary condition, which is indicated with an asterisk and elaborated within this subsection. Dotted lines depict inter-element coupling conditions for poroelastic domains. This finite structure for a halfspace is overlapped with the free field solution of an oblique incident P1-wave, which is reflected along the surface without canyon.

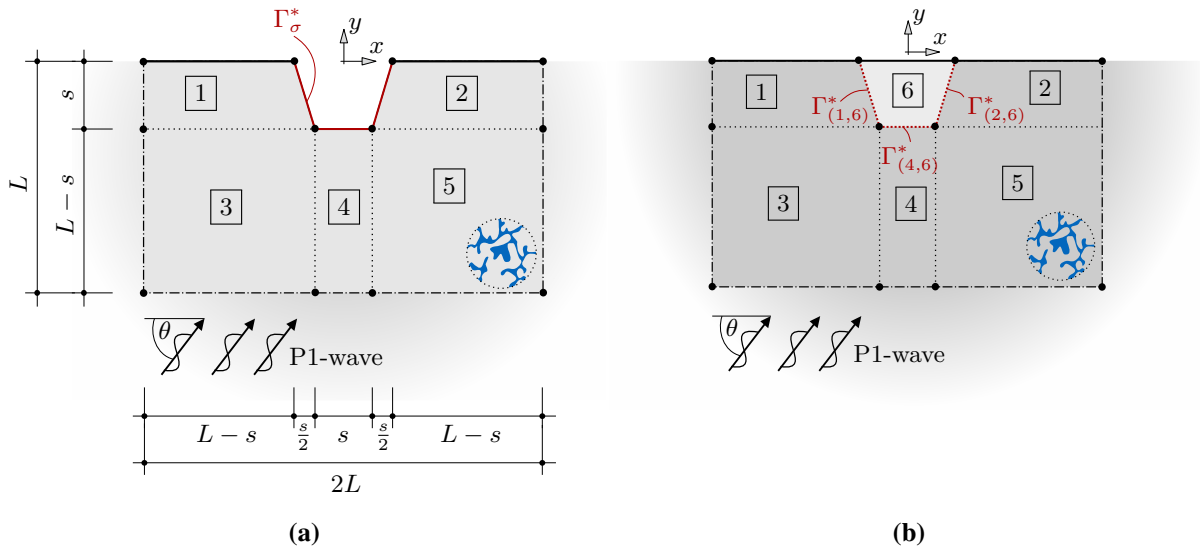


**Figure 2:** WBM model for a halfspace with an empty canyon (a) and a filled canyon (b) exposed to an oblique incident P1-wave

The free field solution  $\mathbf{u}^* = [u_x^*, u_y^*, U_x^*, U_y^*]^T$  is described by the sum of the incident P1-wave and the reflected body waves (P1-, P2-, S-wave), which travel into the halfspace. The incident wave front has the angle  $\theta$  and the amplitude  $I_{p_1}$ . The three reflected body waves have the unknown amplitudes  $R_{p_1}$ ,  $R_{p_2}$  and  $R_s$ .

$$\mathbf{u}^* = \left( I_{p_1} \nabla e^{-ik_{yp_1}y} + R_{p_1} \nabla e^{+ik_{yp_1}y} + R_{p_2} \nabla e^{+ik_{yp_2}y} + R_s \tilde{\nabla} e^{+ik_{ys}y} \right) \cdot e^{-ik_x x} \quad (10)$$

According to *Snell's* law, the horizontal wave number  $k_x = k_{p_1} \cos(\theta)$  of the incident P1-wave remains the same for the reflected P1-, P2- and S-wave. The vertical wave number components are deduced from the physical wave numbers  $k_{p_1}$ ,  $k_{p_2}$  and  $k_s$ .

$$k_{y\bullet} = \sqrt{k_\bullet^2 - k_x^2} \quad \left\{ \begin{array}{l} \Re(k_{y\bullet}) \geq 0 \\ \Im(k_{y\bullet}) \leq 0 \end{array} \right. , \quad \text{with } \bullet \in \{s, p_1, p_2\} \quad (11)$$

The stresses  $\boldsymbol{\sigma}^* = [\sigma_x^*, \sigma_y^*, \tau_{xy}^*, \sigma_f^*]^T$  from the free field solution are derived according to Equation (6), by computing the strain field for the displacements expressed by Equation (10). For an unloaded surface, it must hold that  $[\sigma_y^*, \tau_{xy}^*, \sigma_f^*]^T = [0, 0, 0]^T$ . This permits to set up a system of linear equations, whose unknowns are the amplitudes  $R_{p_1}$ ,  $R_{p_2}$  and  $R_s$ . After computing these, the displacements  $\mathbf{u}^*$  and stresses  $\boldsymbol{\sigma}^*$  for the free field solution are evaluated and involved into the following coupling approach. For a halfspace with canyon, as depicted in Figure 2 (a), the total system response is described as the sum of free field solution ( $\mathbf{u}^*$ ,  $\boldsymbol{\sigma}^*$ ) and scattered wave field ( $\hat{\mathbf{u}}$ ,  $\hat{\boldsymbol{\sigma}}$ ). The scattered wave field is computed with the WBM.

$$\mathbf{u}(\mathbf{r}) \approx \hat{\mathbf{u}}(\mathbf{r}) + \mathbf{u}^*(\mathbf{r}) \quad \boldsymbol{\sigma}(\mathbf{r}) \approx \hat{\boldsymbol{\sigma}}(\mathbf{r}) + \boldsymbol{\sigma}^*(\mathbf{r}) \quad (12)$$

The surface of the empty canyon in Figure 2 (a) is highlighted in red colour and named  $\Gamma_\sigma^*$ . Along this boundary, the scattered and free field are coupled for normal and tangential stresses, indicated with  $\diamond_{n/f}$  and  $\diamond_t$ . The following residuals are formulated for a modified *Neumann* boundary condition. This differs from the formulation in [3], which uses a *Neumann* boundary condition for external stresses  $\bar{\boldsymbol{\sigma}}(\mathbf{r})$  instead of a free field solution  $\boldsymbol{\sigma}^*$ .

$$R_\sigma^*(\mathbf{r}) = \begin{cases} \hat{\sigma}_n(\mathbf{r}) + \sigma_n^*(\mathbf{r}) = 0 \\ \hat{\sigma}_t(\mathbf{r}) + \sigma_t^*(\mathbf{r}) = 0 \\ \hat{\sigma}_f(\mathbf{r}) + \sigma_f^*(\mathbf{r}) = 0 \end{cases} \quad (13)$$

The residuals go through a weighted residual *Galerkin* approach, by weighting them with expressions for normal, tangential and fluid seepage field displacements, which depend on the wave functions of the WBM model. These weighting functions are indicated by  $\tilde{\diamond}$ , so that additional system matrices  $\mathbf{K}_\sigma^{*(\bullet)}$  and load vectors  $\mathbf{f}_\sigma^{*(\bullet)}$  are derived, which contribute to the global system of linear equations. These are set up for each WB element with the domain  $\Omega^{(\bullet)}$ . In the case of a homogeneous halfspace, as depicted in Figure 2 (a), these are the elements  $\boxed{1}$ ,  $\boxed{2}$  and  $\boxed{4}$ , respectively the domains  $\Omega^{(\bullet)}$  with  $\bullet \in \{1; 2; 4\}$ . The parameter  $\mathbf{r} = [x, y]^T$  indicates the position vector.

$$\mathbf{K}_\sigma^{*(\bullet)} = - \int_{\Gamma_\sigma^*} \tilde{\mathbf{u}}_n^{(\bullet)} \cdot \hat{\boldsymbol{\sigma}}_n^{(\bullet)} + \tilde{\mathbf{u}}_t^{(\bullet)} \cdot \hat{\boldsymbol{\sigma}}_t^{(\bullet)} + \frac{1}{n_{f(\bullet)}} \tilde{\mathbf{U}}_f^{(\bullet)} \cdot \hat{\boldsymbol{\sigma}}_f^{(\bullet)} \, d\mathbf{r} \quad (14)$$

$$\mathbf{f}_\sigma^{*(\bullet)} = \int_{\Gamma_\sigma^*} \tilde{\mathbf{u}}_n^{(\bullet)} \cdot \sigma_n^* + \tilde{\mathbf{u}}_t^{(\bullet)} \cdot \sigma_t^* + \tilde{\mathbf{u}}_f \cdot \sigma_f^* + \frac{1}{n_{f(\bullet)}} \tilde{\mathbf{U}}_f^{(\bullet)} \cdot \sigma_f^* \, d\mathbf{r} \quad (15)$$

After solving the final system of linear equations, the response field of the scattered wave field is post-processed on the basis of the computed weighting values and the wave functions. The total system's response is obtained by superposing the field responses from the scattered wave field and the free field, as described by Equation (12).

### 3.2 Modified inter-element coupling conditions

To model a 2D poroelastic halfspace with a filled canyon and incident P1-wave, the problem is divided into a halfspace and canyon region. These are coupled along the boundaries  $\Gamma_{(1,6)}^*$ ,  $\Gamma_{(2,6)}^*$  and  $\Gamma_{(4,6)}^*$ , as indicated in Figure 2 (b). The field response of the halfspace region corresponds to the sum of the free field solution  $\diamond^*$  for an incident P1-wave and the scattered wave field  $\widehat{\diamond}$ . In the following, the total displacements and stresses are expressed for the WB elements  $\boxed{1}$  -  $\boxed{5}$  by superposing the responses  $\diamond^*$  and  $\widehat{\diamond}$ . These elements describe the halfspace region and are represented by the ID  $\alpha \in \{1; 2; 3; 4; 5\}$ .

$$\mathbf{u}^{(\alpha)}(\mathbf{r}) \approx \widehat{\mathbf{u}}^{(\alpha)}(\mathbf{r}) + \mathbf{u}^*(\mathbf{r}) \quad \boldsymbol{\sigma}^{(\alpha)}(\mathbf{r}) \approx \widehat{\boldsymbol{\sigma}}^{(\alpha)}(\mathbf{r}) + \boldsymbol{\sigma}^*(\mathbf{r}) \quad (16)$$

The filled canyon is described by the WB element  $\boxed{6}$ , whose field response corresponds to a scattered wave field. The ID of the WB element is given by  $\beta = 6$ .

$$\mathbf{u}^{(\beta)}(\mathbf{r}) \approx \widehat{\mathbf{u}}^{(\beta)}(\mathbf{r}) \quad \boldsymbol{\sigma}^{(\beta)}(\mathbf{r}) \approx \widehat{\boldsymbol{\sigma}}^{(\beta)}(\mathbf{r}) \quad (17)$$

WB elements, which describe either the halfspace or canyon region, are coupled with compatibility and continuity conditions. These are defined for normal and tangential displacements and stresses, expressed by  $\diamond_{n/f}$  and  $\diamond_t$ .

$$R_{(\alpha,\beta)}^*(\mathbf{r}) = \left\{ \begin{array}{l} \widehat{u}_n^{(\alpha)}(\mathbf{r}) + u_n^*(\mathbf{r}) + \widehat{u}_n^{(\beta)}(\mathbf{r}) = 0 \\ \widehat{u}_t^{(\alpha)}(\mathbf{r}) + u_t^*(\mathbf{r}) + \widehat{u}_t^{(\beta)}(\mathbf{r}) = 0 \\ \widehat{U}_f^{(\alpha)}(\mathbf{r}) + U_f^*(\mathbf{r}) + \widehat{U}_f^{(\beta)}(\mathbf{r}) = 0 \\ \widehat{\sigma}_n^{(\alpha)}(\mathbf{r}) + \sigma_n^*(\mathbf{r}) + \widehat{\sigma}_f^{(\alpha)}(\mathbf{r}) + \sigma_f^*(\mathbf{r}) - \widehat{\sigma}_n^{(\beta)}(\mathbf{r}) - \widehat{\sigma}_f^{(\beta)}(\mathbf{r}) = 0 \\ \widehat{\sigma}_t^{(\alpha)}(\mathbf{r}) + \sigma_t^*(\mathbf{r}) - \widehat{\sigma}_t^{(\beta)}(\mathbf{r}) = 0 \\ \widehat{\sigma}_f^{(\alpha)}(\mathbf{r})/n^{f(\alpha)} + \sigma_f^*(\mathbf{r})/n^{f*} - \widehat{\sigma}_f^{(\beta)}(\mathbf{r})/n^{f(\beta)} = 0 \end{array} \right. \quad (18)$$

A weighted residual *Galerkin* approach is applied to these residuals. System and coupling matrices, as well as load vectors are obtained, which contribute to the final system of linear equations.

$$\mathbf{K}^{(\alpha,\alpha)} = \int_{\Gamma_{(\alpha,\beta)}} \widetilde{\boldsymbol{\sigma}}_n^{(\alpha)} \widehat{\mathbf{u}}_n^{(\alpha)\top} + \widetilde{\boldsymbol{\sigma}}_t^{(\alpha)} \widehat{\mathbf{u}}_t^{(\alpha)\top} + \frac{1}{n^{f(\alpha)}} \widetilde{\boldsymbol{\sigma}}_f^{(\alpha)} \widehat{\mathbf{U}}_f^{(\alpha)\top} \mathrm{d}\mathbf{r} \quad (19)$$

$$\mathbf{C}^{(\alpha,\beta)} = \int_{\Gamma_{(\alpha,\beta)}} \tilde{\boldsymbol{\sigma}}_n^{(\alpha)} \widehat{\mathbf{u}}_n^{(\beta)\text{T}} + \tilde{\boldsymbol{\sigma}}_t^{(\alpha)} \widehat{\mathbf{u}}_t^{(\beta)\text{T}} + \frac{1}{n^{f(\alpha)}} \tilde{\boldsymbol{\sigma}}_f^{(\alpha)} \widehat{\mathbf{U}}_f^{(\beta)\text{T}} \, \text{d}\mathbf{r} \quad (20)$$

$$\mathbf{K}^{(\beta,\beta)} = \int_{\Gamma_{(\alpha,\beta)}} \tilde{\mathbf{u}}_n^{(\beta)} \widehat{\boldsymbol{\sigma}}_n^{(\beta)\text{T}} + \tilde{\mathbf{u}}_n^{(\beta)} \widehat{\boldsymbol{\sigma}}_f^{(\beta)\text{T}} + \tilde{\mathbf{u}}_t^{(\beta)} \widehat{\boldsymbol{\sigma}}_t^{(\beta)\text{T}} + \frac{1}{n^{f(\beta)}} \tilde{\mathbf{U}}_f^{(\beta)} \widehat{\boldsymbol{\sigma}}_f^{(\beta)\text{T}} \, \text{d}\mathbf{r} \quad (21)$$

$$\mathbf{C}^{(\beta,\alpha)} = - \int_{\Gamma_{(\alpha,\beta)}} \tilde{\mathbf{u}}_n^{(\beta)} \widehat{\boldsymbol{\sigma}}_n^{(\alpha)\text{T}} + \tilde{\mathbf{u}}_n^{(\beta)} \widehat{\boldsymbol{\sigma}}_f^{(\alpha)\text{T}} + \tilde{\mathbf{u}}_t^{(\beta)} \widehat{\boldsymbol{\sigma}}_t^{(\alpha)\text{T}} + \frac{1}{n^{f(\alpha)}} \tilde{\mathbf{U}}_f^{(\beta)} \widehat{\boldsymbol{\sigma}}_f^{(\alpha)\text{T}} \, \text{d}\mathbf{r} \quad (22)$$

$$\mathbf{f}^{*(\alpha)} = - \int_{\Gamma_{(\alpha,\beta)}^*} \tilde{\boldsymbol{\sigma}}_n^{(\alpha)} u_n^* + \tilde{\boldsymbol{\sigma}}_t^{(\alpha)} u_t^* + \frac{1}{n^{f(\alpha)}} \tilde{\boldsymbol{\sigma}}_f^{(\alpha)} U_f^* \, \text{d}\mathbf{r} \quad (23)$$

$$\mathbf{f}^{*(\beta)} = \int_{\Gamma_{(\alpha,\beta)}^*} \tilde{\mathbf{u}}_n^{(\beta)} \sigma_n^* + \tilde{\mathbf{u}}_n^{(\beta)} \sigma_f^* + \tilde{\mathbf{u}}_t^{(\beta)} \sigma_t^* + \frac{1}{n^{f^*}} \tilde{\mathbf{U}}_f^{(\beta)} \sigma_f^* \, \text{d}\mathbf{r} \quad (24)$$

After the computation of the weighting values for the wave functions of the WBM model, the system's response is post-processed. Displacements and stresses within the halfspace are evaluated according to Equation (16), which describe the superposition of the scattered and free field solution. The field responses for the filled canyon are post-processed with the weighted wave functions of the related WB element(s), compare also Equation (17).

## 4 NUMERICAL EXAMPLES

### 4.1 Empty canyon: Comparison with results from literature

Given is a poroelastic halfspace with a trapezoidal canyon, as depicted in Figure 2 (a) with  $s = 10$  m and  $L \in \{20 \text{ m}; 40 \text{ m}\}$ . The material of the soil is a sandstone, as described in [8], whereby the porosity is assumed to be very small ( $n^f = 0.01$ ) for the following numerical example. The material values are summarized in Table 1, in which the adapted parameters are indicated with an asterisk. With these adaptations, the poroelastic model tends to the state of an elastic model, which permits to compare the simulation results with the solution provided by [9]. In this publication, different canyon geometries are observed for an elastic halfspace with a wave velocity ratio of  $c_s/c_{p_1} = 2.0$  and a normalized frequency  $f_n = 2sf \cdot \sqrt{(\rho/\mu)} = 2.0$ . For the WBM model, this normalized frequency corresponds to an excitation frequency of  $f = 223.27$  Hz

For this model, the vertical and horizontal displacement amplitudes are evaluated along the surface of the halfspace ( $x \in ] - \infty; -10 \text{ m}[ \cup ]10 \text{ m}; +\infty[$ ) and the empty canyon ( $x \in [-10 \text{ m}; 10 \text{ m}]$ ). The dimension  $L$  and the incidence angle  $\theta$  are varied, and take the values  $L \in \{30 \text{ m}; 60 \text{ m}\}$  and  $\theta \in \{30^\circ; 60^\circ; 90^\circ\}$ . The amplitude of the oblique incident P1-wave is given as  $I_{p_1} = A_{p_1}/k_{p_1}$ , with an arbitrary value  $A_{p_1} \in \mathbb{R}/\{0\}$ . The plots in Figure 3 present the computed displacement amplitudes, which are normalized w.r.t.  $A_{p_1}$ , together with the reference solution by [9]. In general, it can be seen that the WBM model with  $L = 40$  m delivers

**Table 1:** Material parameters for water saturated sandstone [8] and Molsand soil [7]

Symbol	Sandstone	Molsand	Definition
$n^f$	0.01*	0.388	porosity
$\rho_f$	1000 kg/m <sup>3</sup>	1000 kg/m <sup>3</sup>	density, water
$\rho_s$	2650 kg/m <sup>3</sup>	2650 kg/m <sup>3</sup>	density, solid matrix
$\rho$	2633.5 kg/m <sup>3</sup>	2009.8 kg/m <sup>3</sup>	density, mixture
$\nu$	0.30	0.333	<i>Poisson's</i> coefficient
$k_c$	[10 <sup>-6</sup> ; 10 <sup>-2</sup> ] m/s	[8 · 10 <sup>-5</sup> ; 10 <sup>-3</sup> ] m/s	hydraulic conductivity
$\eta$	0.02**	0.05	loss factor, drained rock
$E$	3.50 · 10 <sup>10</sup> N/m <sup>2</sup> *	2.98 · 10 <sup>8</sup> N/m <sup>2</sup>	<i>Young's</i> modulus, drained rock
$\alpha$	0.0276*	1.0	1st <i>Biot</i> coefficient
$M$	1.82 · 10 <sup>11</sup> N/m <sup>2</sup> *	5.67 · 10 <sup>9</sup> N/m <sup>2</sup>	2nd <i>Biot</i> coefficient
$a_t$	1.0*	1.0	tortuosity

\* These values are adapted so that the poroelastic medium tends to the state of an elastic medium.

\*\* This value is chosen to decrease the effect of spurious reflections along the absorbing boundaries of the numerical model.

adequate results, which are very close to the reference data. For a smaller model size  $L = 20$  m, the WBM shows less accurate results. This is related to the effect of spurious reflections along the absorbing boundaries, which just permit the perfect absorption of normal incident wave fronts. As the incident P1-wave from the free field is reflected along the edges of the empty canyon, P- and S-waves travel into the halfspace. These wave fronts are not necessarily perpendicular to the absorbing boundaries of the WBM model and get reflected. To reduce the effect of these spurious reflections, the dimension  $L$  of the WBM model is increased, so that waves traveling between canyon and absorbing boundaries are stronger damped.

## 4.2 Filled canyon: Comparison with an analytical solution

The coupling conditions, introduced in Section 3.2, are tested against the analytical solution for a halfspace with filled canyon, whereby halfspace and canyon have the same material. Figure 2 (b) presents a poroelastic halfspace ( $L = 50$  m,  $s = 10$  m) with a filled canyon, both with Molsand soil as described by [7]. The WBM model, consisting of six elements, is tested for an increasing number of wave functions. The incident wave front is chosen to be a P1-wave with the angle of incidence  $\theta = 60^\circ$  and the frequency  $f = 100$  Hz. The hydraulic conductivity  $k_c$  is varied w.r.t. the dimensionless frequency  $\chi \in \{0.01; 1.0; 100\}$ , which is defined as:

$$\chi = \frac{\omega}{\omega_0} = 2\pi f \cdot \left( \frac{\rho n^f}{k_c (\rho a_t - \rho_f n^f)} \cdot 9.81 \text{ m/s}^2 \right)^{-1} \quad (25)$$

According to [10], the phase velocities and the attenuation of the three body waves (P1, P2, S) increase in a range of  $0.1 < \chi < 10$ . As shown for example in [7], this is also the range,

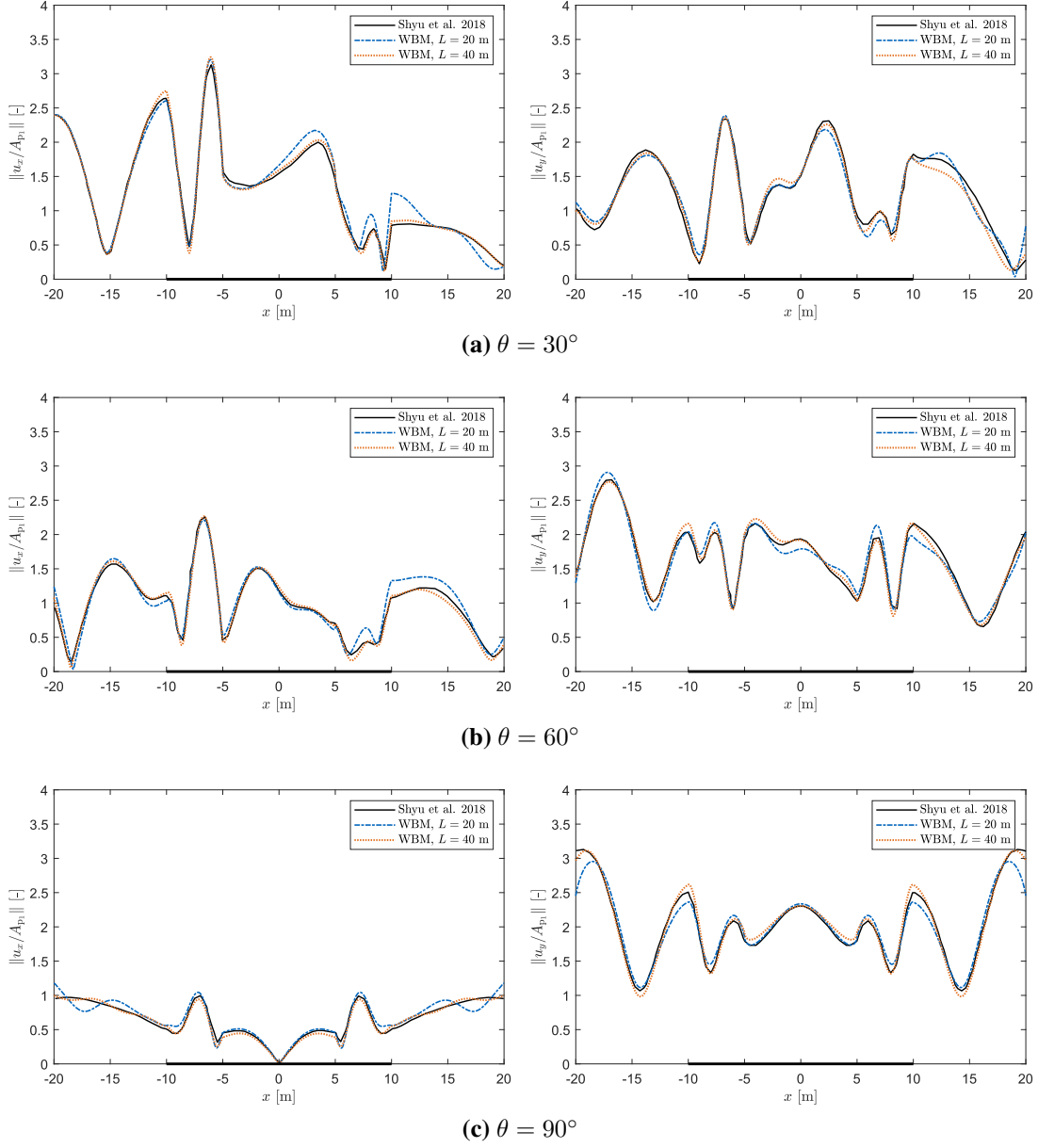


**Figure 3:** Displacement amplitudes along the surface of a halfspace ( $c_s/c_{p1} = 2.0$ ) with an empty canyon for an oblique incident P1-wave and different angles of incidence  $\theta$  **(a) - (c)**

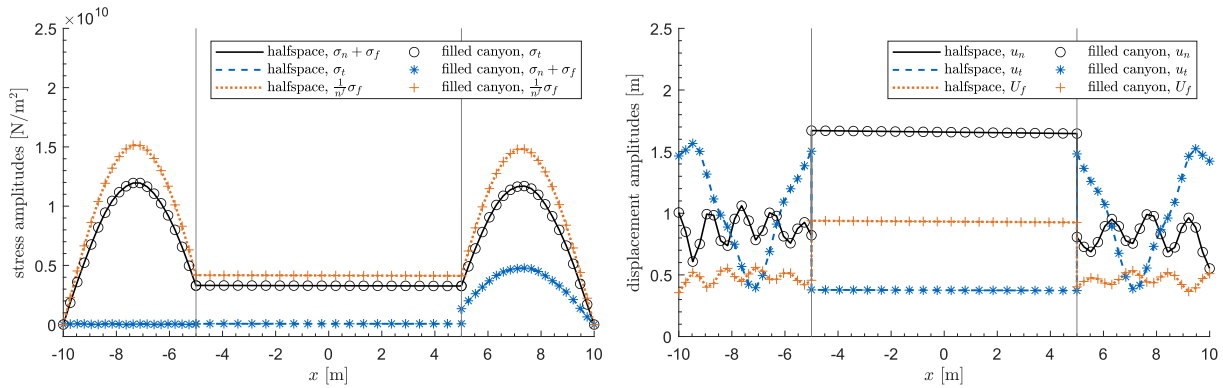


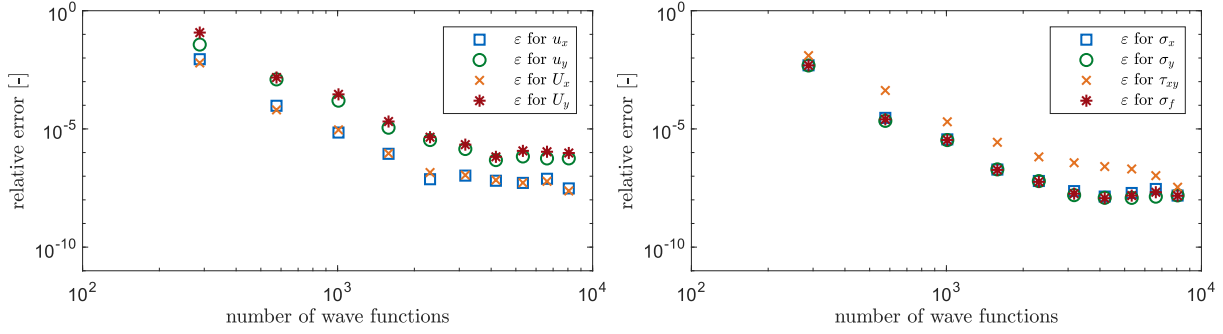
**Figure 4:** Evaluated coupling conditions from Equation (18) between the canyon and halfspace domains

for which the strongest effect of viscous damping is retrieved. Beyond that range, the porous continuum tends either to a state of loose coupling between fluid and solid phase ( $\chi \gg 10$ ) or to very strong coupling ( $\chi \ll 0.1$ ), for which the medium is often described as a frozen mixture. To check the influence from viscous damping on the performance of the WBM model and its convergence towards the analytical solution, a very low, medium and a very high value for  $\chi$  are chosen. For each value of the dimensionless frequency, the hydraulic conductivity  $k_c$  is recomputed from Equation (25) and the number of wave functions is continuously increased, so that the following averaged relative errors are evaluated.

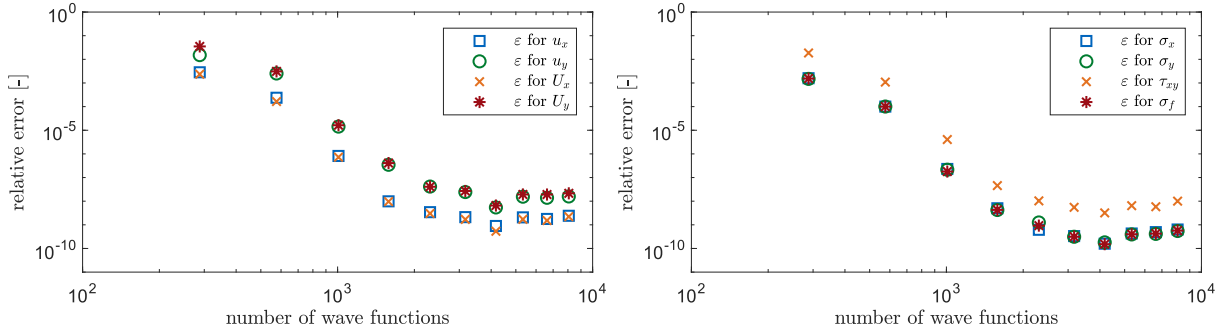
$$\epsilon_{\diamond} = \frac{1}{n_{\text{OP}}} \cdot \sum_{i=1}^{n_{\text{OP}}} \frac{\|\diamond - \diamond_{\text{ref}}\|}{\|\diamond_{\text{ref}}\|}, \quad \text{with } n_{\text{OP}} = 5 \quad (26)$$

The relative errors are computed for all field variables, indicated with  $\diamond \in \{u_x, u_y, U_x, U_y, \sigma_x, \sigma_y, \tau_{xy}, \sigma_f\}$ . The reference solution corresponds to the analytical solution for an incident P1-wave, which is reflected along an unloaded surface. The relative errors are averaged for five points with the coordinates  $(x|y)$ :  $(-30|-20)$ ,  $(0|-15)$ ,  $(15|-22)$ ,  $(25|-5)$ ,  $(-2|-5)$ .

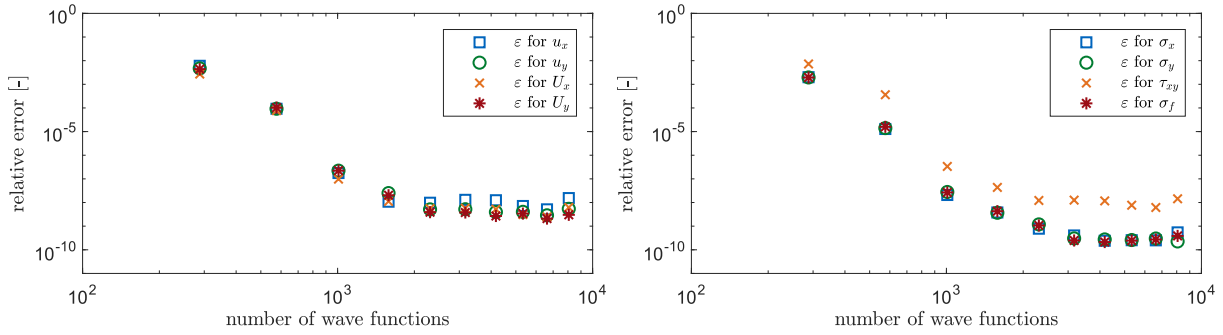
The diagrams in Figure 5 present the evaluated errors and indicate an overall convergence for more than 2000 wave functions. The errors lie in a range of  $10^{-10}$  to  $10^{-6}$  and show a good agreement between the WBM model and the analytical solution. To illustrate the successful coupling between canyon and halfspace, respectively between the elements  $\boxed{6}$  and  $\boxed{1}$ ,  $\boxed{2}$ ,  $\boxed{4}$ , normal and tangential field variables are plotted in Figure 4. For these plots, a WBM model with 8064 wave functions and  $\chi = 100$  is chosen. The diagrams depict the coupled displacements and stresses, compare also Equation (18), which are evaluated along the coupled boundaries  $\Gamma_{(1,6)}^*$ ,  $\Gamma_{(2,6)}^*$  and  $\Gamma_{(4,6)}^*$ . The computed responses are illustrated with respect to the global  $x$ -coordinate. Due to this,  $x \in [-10; -5]$  m and  $x \in [5; 10]$  m correspond to the left and right inclined edges of the canyon, whereas  $x \in [-5; -5]$  m describes its lower edge.



(a)  $\chi = 0.01$



(b)  $\chi = 1.0$



(c)  $\chi = 100$

**Figure 5:** Averaged relative errors for different dimensionless frequencies  $\chi$  (a) - (c)

## 5 CONCLUSIONS

Within this paper, two coupling approaches are presented to extend the WBM to the analysis of scattered wave fields due to oblique incident wave fronts. These coupling approaches are specifically elaborated for empty and filled canyons and are applied to poroelastic media. In a first step, numerical examples are presented to compare the accuracy and performance of this method with a reference from literature and an analytical solution. The next step will be, to test these approaches against further examples from literature, to discuss the effect of poroelasticity and to use the computational benefits from the WBM by extending it to the time domain.

## REFERENCES

- [1] Dravinski, M. and Mossessian, T.K. Scattering of plane harmonic P, SV, and Rayleigh waves by dipping layers of arbitrary shape. *Bull. Seismol. Soc. Am.* (1987) **77**:212–235.
- [2] Sánchez-Sesma, F.J. and Campillo, M. Diffraction of P, SV, and Rayleigh waves by topographic features: A boundary integral formulation. *Bull. Seismol. Soc. Am.* (1991) **81**(6):2234–2253.
- [3] Lainer, M. and Taddei, F. and Müller, G. A Wave Based Method for the analysis of a fully and partially saturated halfspace under harmonic loading. *Comput. Struct.* (2023) **283**:107040.
- [4] Desmet, W. *A wave based prediction technique for coupled vibro-acoustic analysis*, PhD. thesis 98D12. Faculteit Toegepaste Wetenschappen, Katholieke Universiteit Leuven (1998).
- [5] Biot, M.A. Mechanics of deformation and acoustic propagation in porous media. *J. Appl. Phys.* (1962) **33**(4):1482–1498.
- [6] Deckers, E. *A wave based approach for steady-state Biot models of poroelastic materials*, PhD. thesis 2012D12. Faculty of Engineering, Katholieke Universiteit Leuven (2012).
- [7] Degrande, G. *A spectral and finite element method for wave propagation in dry and saturated poroelastic media*, PhD Thesis. Katholieke Universiteit Leuven (1992).
- [8] Lin, C.H. and Lee, V.W. and Trifunac, M.D. The reflection of plane waves in a poroelastic half-space saturated with inviscid fluid. *Soil Dyn. Earthq. Eng.* (2005) **25**(3):205–223.
- [9] Shyu, W.-S. and Teng, T.-J. and Chou, C.-S. Effect of geometry on in-plane responses of a symmetric canyon subjected by P waves. *Soil Dyn. Earthq. Eng.*, **113** (2018) 215–229.
- [10] Atkin, R.J. Completeness theorems for linearized theories of interacting continua. *Quart. Journ. Mech. and Applied Math.* (1968) **21**(2):171–193.